J Mater Sci (2007) 42:8178–8188
DOI 10.1007/s10853-007-1700-0

Growth rate of Nb_3Sn for reactive diffusion between Nb and Cu–9.3Sn–0.3Ti alloy

Ken-ichiro Mikami · Masanori Kajihara

Received: 23 December 2006 / Accepted: 15 March 2007 / Published online: 9 June 2007

Abstract In order to examine experimentally the growth behavior of Nb_3Sn during reactive diffusion between Nb and a bronze with the $\alpha + \beta$ two-phase microstructure, a sandwich (Cu–Sn–Ti)/Nb/(Cu–Sn–Ti) diffusion couple was prepared from pure Nb and a ternary Cu–Sn–Ti alloy with concentrations of 9.3 at.% Sn and 0.3 at.% Ti by a diffusion bonding technique. Here, α is the primary solid-solution phase of Cu with the face-centered cubic structure, and β is the intermediate phase with the body-centered cubic structure. The diffusion couple was isothermally annealed at temperatures between $T = 923$ and 1,053 K for various times up to 843 h. Owing to annealing, the Nb_3Sn layer is formed along each (Cu–Sn–Ti)/Nb interface in the diffusion couple, and grows mainly into Nb. Hence, the migration of the Nb_3Sn/Nb interface governs the growth of the Nb_3Sn layer. The mean thickness of the Nb_3Sn layer is proportional to a power function of the annealing time. The exponent of the power function is close to unity at $T = 923$ K, but takes values of 0.8–0.7 at $T = 973$–1,053 K. Consequently, the interface reaction at the migrating Nb_3Sn/Nb interface is the rate-controlling process for the growth of the Nb_3Sn layer at $T = 923$ K, and the interdiffusion across the Nb_3Sn layer as well as the interface reaction contributes to the rate-controlling process at $T = 973$–1,053 K. Except the effect of Ti, the growth rate of the Nb_3Sn layer is predominantly determined by the activity of Sn in the bronze and thus the concentration of Sn in the α phase. As a result, the growth rate is hardly affected by the volume fraction of the β phase, though the final amount of the Nb_3Sn layer may depend on the volume fraction.

K. Mikami
Graduate School, Tokyo Institute of Technology, Yokohama 226-8502, Japan

M. Kajihara (✉)
Department of Materials Science and Engineering, Tokyo Institute of Technology, Yokohama 226-8502, Japan
e-mail: kajihara@materia.titech.ac.jp

Introduction

In electronic industry, a bronze method has been conveniently used to manufacture superconducting Nb_3Sn composite-wires with multifilamentary structure [1–12]. Here, Nb_3Sn is an intermetallic compound with the A-15 type crystal structure. In the bronze method, a ductile rod of Nb is embedded in a Cu–Sn alloy matrix and then extruded into a filament form. The resultant multifilamentary wire is annealed at an adequate temperature. Owing to reactive diffusion during annealing, a layer of Nb_3Sn is produced at the interface between the Cu–Sn alloy and Nb. The Cu–Sn alloy is called bronze, and hence this technique is denominated the bronze method. The growth behavior of the Nb_3Sn layer in the bronze method was investigated by many researchers [5–12]. However, monofilamentary and multifilamentary diffusion couples were adopted in most of the investigations. In such diffusion couples, interdiffusion occurs in rather complicated manners, and thus the Nb_3Sn layer with a uniform thickness cannot be formed easily. Consequently, the filamentary diffusion couples are not appropriate to observe the growth behavior of the Nb_3Sn layer.

Instead of the filamentary diffusion couples, sandwich (Cu–Sn)/Nb/(Cu–Sn) diffusion couples were used to study experimentally the growth behavior of the Nb_3Sn layer in the bronze method [13, 14]. In the sandwich diffusion

couple, interdiffusion takes place along the direction perpendicular to the interface, and hence the Nb_3Sn layer with a rather uniform thickness is formed during the interdiffusion. In the experiment by Osamura et al. [13], a sandwich diffusion couple was prepared from pure Nb and a binary Cu–Sn alloy containing 7.4 at.% of Sn, and then isothermally annealed in the temperature range between $T = 973$ and 1,073 K. A different sandwich diffusion couple was prepared from pure Nb and a binary Cu–Sn alloy with a concentration of 8.3 at% Sn in a previous experimental study [14]. In that experiment, the isothermal annealing was carried out at $T = 923$–1,053 K. During annealing, a layer of Nb_3Sn with an almost uniform thickness is actually produced along the (Cu–Sn)/Nb interface in the sandwich diffusion couple, and grows mainly into Nb. The mean thickness of the Nb_3Sn layer is expressed as a power function of the annealing time. For the Cu–8.3Sn diffusion couple, the exponent of the power function is nearly equal to unity at $T = 923$–973 K, and monotonically decreases from 1 to 0.8 with increasing annealing temperature from $T = 973$ K to $T = 1{,}053$ K. This means that interface reaction predominantly controls the growth rate of the Nb_3Sn layer at $T = 923$–973 K and interdiffusion contributes to the rate-controlling process at $T = 973$–1,053 K.

In order to improve the superconducting properties of Nb_3Sn, a small amount of Ti is added to the Cu–Sn alloy. Influence of Ti on the growth of the Nb_3Sn layer was experimentally studied by Osamura et al. at $T = 973$–1,073 K using a sandwich (Cu–Sn–Ti)/Nb/(Cu–Sn–Ti) diffusion couple with concentrations of 7.5 at.% Sn and 1 at.% Ti [13]. The influence of Ti was also experimentally examined at $T = 923$–1,053 K using a sandwich diffusion couple with concentrations of 8.1 at.% Sn and 0.3 at.% Ti in a previous study [15]. According to the experimental result for the Cu–8.1Sn–0.3Ti diffusion couple [15], the addition of Ti into the Cu–Sn alloy considerably accelerates the growth of the Nb_3Sn layer at higher annealing temperatures but hardly at lower annealing temperatures. Thus, the influence of Ti varies depending on the annealing temperature. Also in this case, the mean thickness of the Nb_3Sn layer is described as a power function of the annealing time. Furthermore, the temperature dependence of the exponent of the power function is almost equivalent between the Cu–8.3Sn and Cu–8.1Sn–0.3Ti diffusion couples. This implies that the same rate-controlling process works for the reactive diffusion in these diffusion couples.

Recently, Cu–Sn alloys with the $\alpha + \beta$ two-phase microstructure are preferentially used to manufacture the superconducting Nb_3Sn composite-wire. Here, α is the primary solid-solution phase of Cu with the face-centered cubic structure, and β is the intermediate phase with the body-centered cubic structure. In the binary Cu–Sn system [16], the α phase is stable up to the melting temperature of $T = 1{,}358$ K for pure Cu, but the β phase is merely stable at $T = 859$–1,071 K. The solubility of Sn in the α phase is 9.1 and 7.7 at.% at $T = 859$ and 1,071 K, respectively, and the solubility range of the β phase is 13.1–16.5 at.% Sn at $T = 859$–1,071 K. Since the concentration of Sn is higher in the β phase than in the α phase, the amount of Sn supplied to the Nb_3Sn layer is greater for the Cu–Sn alloy with the $\alpha + \beta$ two-phase microstructure than for that with the α single-phase microstructure. Hence, we may expect that the growth rate of the Nb_3Sn layer monotonically increases with increasing volume fraction of the β phase in the Cu–Sn alloy. Unfortunately, however, reliable information for influence of the β phase on the growth of the Nb_3Sn layer is not available. In the present study, the growth behavior of the Nb_3Sn layer was experimentally examined using a sandwich (Cu–Sn–Ti)/Nb/(Cu–Sn–Ti) diffusion couple composed of a Cu–9.3Sn–0.3Ti alloy and pure Nb. The diffusion couple was isothermally annealed at temperatures of $T = 923$–1,053 K. At these temperatures, the $\alpha + \beta$ two-phase microstructure is realized in the Cu–9.3Sn–0.3Ti alloy. The mean thickness of the Nb_3Sn layer produced in the diffusion couple during annealing was observed in a metallographical manner. The experimental result of the Cu–9.3Sn–0.3Ti diffusion couple was compared with those of the Cu–8.3Sn and Cu–8.1Sn–0.3Ti diffusion couples reported in previous studies [14, 15]. The rate-controlling process for the growth of the Nb_3Sn layer was discussed on the basis of the comparison.

Experimental

Plate specimens with a dimension of 2 mm × 5 mm × 12 mm were prepared by spark erosion from a hot-rolled rectangular ingot of a ternary Cu–9.3 at.% Sn–0.3 at.% Ti alloy in a manner similar to previous studies [14, 15]. Parallel surfaces with an area of 5 mm × 12 mm of each Cu–Sn–Ti plate specimen were mechanically polished on 120–800 emery papers. One of the polished parallel-surfaces was again mechanically polished on 1,500–4,000 emery papers, and then finished using diamond with a size of 1 μm. A pure Nb specimen with a dimension of 1 mm × 10 mm × 10 mm and purity of 99.9 % was cold rolled to a thickness of 0.1 mm. Sheet specimens with a size of 0.1 mm × 5 mm × 12 mm were cut from the cold-rolled Nb specimen, and then degreased in acetone with an ultrasonic cleaner.

After degreasing, a Nb sheet specimen was immediately sandwiched between the finished surfaces of two freshly prepared Cu–Sn–Ti plate specimens in ethanol by a technique adopted in a previous study [17]. Each (Cu–Sn–Ti)/Nb/(Cu–Sn–Ti) couple was completely dried, and then

isothermally heat-treated for diffusion bonding in an evacuated silica tube, followed by air-cooling. The diffusion bonding was carried out at temperatures of T = 923 and 973 K for 5 h and at those of T = 1,023 and 1,053 K for 3 h. The diffusion couples were separately encapsulated in evacuated silica capsules, and then isothermally annealed at T = 923, 973, 1,023 and 1,053 K for various times up to 838 h. Hereafter, the summation of the heat-treating and annealing times is merely called the annealing time t. Cross-sections of the annealed diffusion couple were mechanically polished using 1,500–4,000 emery papers and diamond with a size of 1 μm, and then finished with an OP-S liquid by Struers Ltd. The microstructure of the cross-section was observed with a backscattered electron image (BEI) by scanning electron microscopy (SEM). Concentration profiles of Cu, Nb, Sn and Ti for various phases on the cross-section were measured by electron probe microanalysis (EPMA).

Results and discussion

Microstructure

A typical BEI micrograph for the cross-section of the annealed diffusion couple is shown in Fig. 1. This figure indicates the micrograph for the Cu–Sn–Ti alloy slightly away from the Nb specimen in the diffusion couple with an annealing temperature of T = 1,053 K and an annealing time of t = 21 h (7.56×10^4 s). As can be seen in Fig. 1, the Cu–Sn–Ti alloy consists of two phases with dark and bright contrasts. The dark and bright phases are the α and β phases, respectively. Here, α is the primary solid-solution phase of Cu with the face-centered cubic (fcc) structure, and β is the intermediate phase with the body-centered cubic (bcc) structure. According to the micrograph in Fig. 1, the β phase is rather irregular in morphology. Furthermore, small grains of the α phase are distributed in the β phase. Concentration profiles of the constituent components in the α and β phases were measured by EPMA. The measurement was carried out for the β phase with less grains of the α phase. A typical result is shown in Fig. 2. In this figure, the ordinate and the abscissa indicate the mol fraction y_i of component i and the distance x, respectively, and open squares and rhombuses show the values of y_{Sn} and y_{Ti}, respectively. As can be seen in Fig. 2, y_{Ti} is very small in both the α and β phases. Thus, the Cu–9.3Sn–0.3Ti alloy is approximately considered as the binary Cu–9.3Sn alloy. According to a recent phase diagram in the binary Cu–Sn system [16], the equilibrium compositions $y_{Sn}^{\alpha\beta}$ and $y_{Sn}^{\beta\alpha}$ for the α and β phases of the α + β two-phase tie-line varies from 0.091 and 0.149, respectively, at T = 859 K to 0.077 and 0.131, respectively, at T = 1,071 K [16]. Hence, the overall composition of the Cu–9.3Sn alloy is located in the α + β two-phase region at T = 859–1,071 K. The α + β two-phase microstructure of the Cu–Sn–Ti alloy was actually observed for all the diffusion couples annealed at T = 923–1,053 K. The values $y_{Sn}^{\alpha\beta}$ = 0.078 and $y_{Sn}^{\beta\alpha}$ = 0.135 for T = 1,053 K are indicated as horizontal solid lines in the α and β phases, respectively, in Fig. 2. As can be seen, the open squares are located rather well on the solid line in the α phase, but slightly scattered and located on the upper side of the solid line in the β phase. As mentioned in Sect. ''Experimental'', the Cu–Sn–Ti alloy was merely prepared

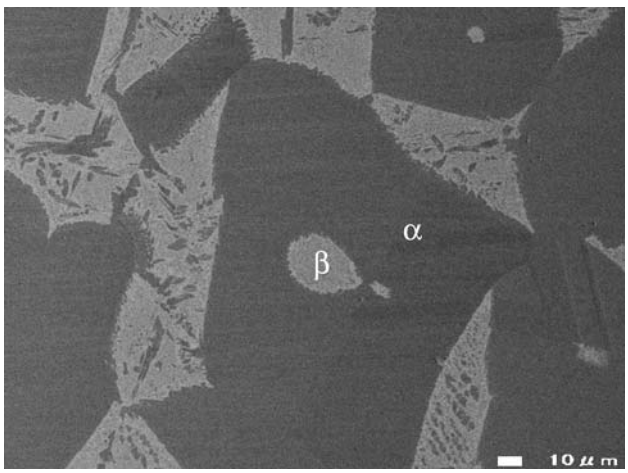

Fig. 1 Back-scattered electron image of cross-section for the Cu–9.3Sn–0.3Ti alloy in the diffusion couple annealed at T = 1,053 K for t = 21 h (7.56×10^4 s)

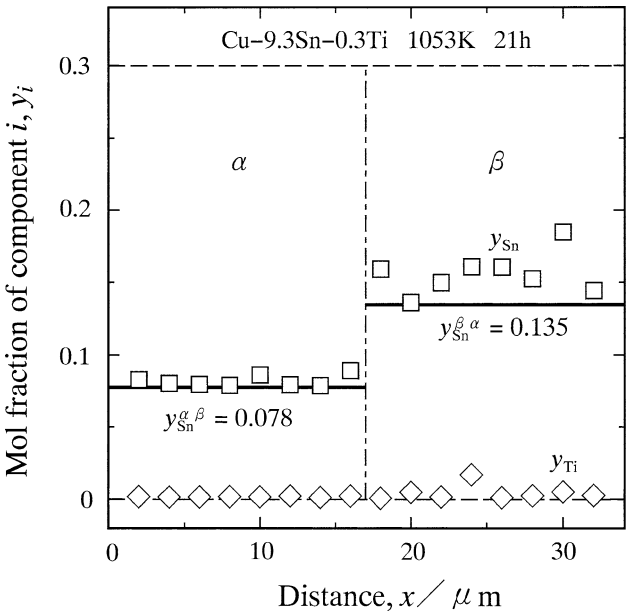

Fig. 2 Concentration profiles of Sn and Ti in the α and β phases for Fig. 1

from the hot-rolled rectangular ingot. Therefore, even after annealing for t = 21 h (7.56×10^4 s) at T = 1,053 K, the equilibrium may not be realized in the Cu–Sn–Ti alloy. This is the reason why the values of y_{Sn} for the β phase are slightly scattered and greater than $y_{Sn}^{\beta\alpha}$ in Fig. 2.

Figure 3 shows a BEI micrograph for the Nb specimen on the cross-section of the same diffusion couple as Fig. 1. As can be seen in Fig. 3, an intermetallic compound layer with the most bright contrast is discerned at each (Cu–Sn–Ti)/Nb interface. This compound layer is Nb_3Sn. The total thickness of the two Nb_3Sn layers and the Nb specimen is close to the initial thickness of 0.1 mm for the Nb specimen, though the thickness of the Nb_3Sn layer becomes about 30 μm due to annealing. This indicates that the Nb_3Sn layer grows mainly into the Nb specimen but hardly towards the Cu–Sn–Ti alloy. Such growth behavior of the Nb_3Sn layer was observed for all the annealed diffusion couples. According to the micrograph in Fig. 3, the β phase is not recognized in the Cu–Sn–Ti alloy neighboring the Nb_3Sn layer. Concentration profiles of the constituent components across the Nb_3Sn layer were determined by EPMA along the direction normal to the interface. A typical result for the diffusion couple in Fig. 3 is indicated in Fig. 4. In this figure, the ordinate and the abscissa show the mol fraction y_i and the distance x, respectively, and open circles, triangles, squares and rhombuses indicate the values of y_{Cu}, y_{Nb}, y_{Sn} and y_{Ti}, respectively. As can be seen, y_{Cu} monotonically decreases from the α phase of the Cu–Sn–Ti alloy to the Nb specimen, and y_{Nb} from the Nb specimen to the α phase. On the other hand, y_{Sn} is greater in the Nb_3Sn layer than in the α phase. Such a tendency is observed also for y_{Ti}, though the difference of y_{Ti} is rather small between the Nb_3Sn layer and the α phase. This means that the uphill diffusion of Sn and Ti occurs from the α phase to the Nb_3Sn layer.

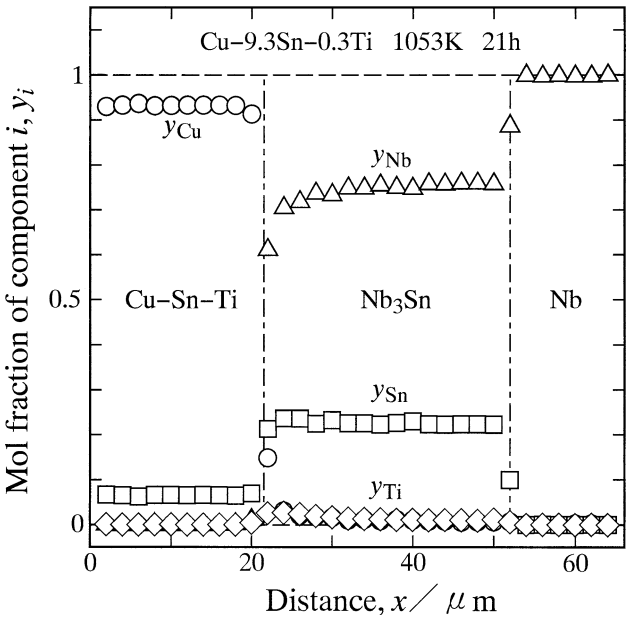

Fig. 4 Concentration profiles of Cu, Nb, Sn and Ti across the Nb_3Sn layer in Fig. 3

A BEI micrograph of a region covering the Nb specimen and the $\alpha + \beta$ two-phase area on the cross-section of the same diffusion couple as Figs. 1 and 3 is indicated in Fig. 5. In this figure, the Nb specimen is located on the lower side, and the $\alpha + \beta$ two-phase area lies on the upper side. As can be seen in Fig. 5, an area with the α single-phase microstructure is formed between the Nb_3Sn layer and the $\alpha + \beta$ two-phase area. Although the β phase is rather irregular in morphology, the base-line of the α single-phase area shown as a dotted line is almost parallel to the α/Nb_3Sn interface. Thus, the mean thickness of the α single-phase area is defined as the distance d between the base-line and the α/Nb_3Sn interface. According to the

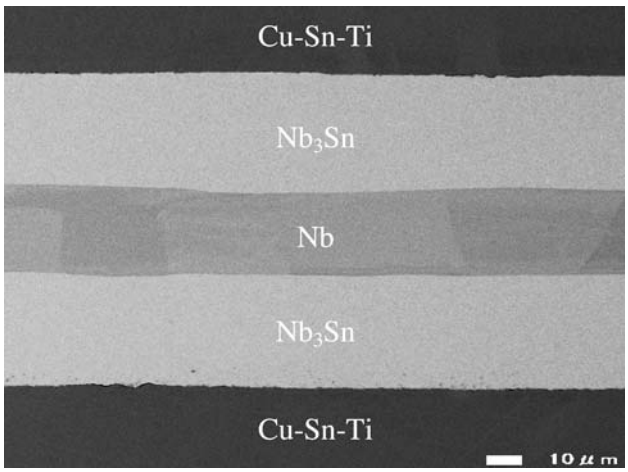

Fig. 3 Back-scattered electron image of cross-section for the Nb specimen in the diffusion couple of Fig. 1

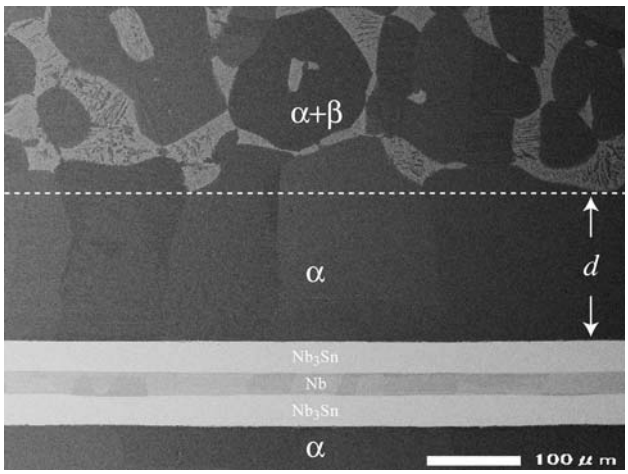

Fig. 5 Back-scattered electron image of cross-section for the diffusion couple of Figs. 1 and 3

micrograph in Fig. 5, d is about 140 μm. Concentration profiles of the constituent components across the α single-phase area along the direction normal to the α/Nb_3Sn interface were determined by EPMA. A typical result for the diffusion couple in Fig. 5 is indicated in Fig. 6. In this figure, the ordinate shows the mol fraction y_i, and the abscissa indicates the distance x measured from the α/Nb_3Sn interface. A vertical dashed-and-dotted line shows the position $x = d$ for the base-line of the α single-phase area, and a horizontal solid line indicates the solubility $y_{Sn}^{\alpha\beta} = 0.078$ of Sn in the α phase at $T = 1{,}053$ K [16]. As can be seen in Fig. 6, the concentration y_{Sn} of Sn in the α phase is smaller than $y_{Sn}^{\alpha\beta}$ in the vicinity of the α/Nb_3Sn interface, but close to $y_{Sn}^{\alpha\beta}$ in the neighborhood of the base-line. Furthermore, y_{Sn} monotonically decreases with decreasing distance at $x < d$. This means that diffusion of Sn occurs across the α single-phase area from the $\alpha + \beta$ two-phase area to the Nb_3Sn layer.

Growth behavior of Nb_3Sn layer

In the BEI micrograph of the cross-section like Fig. 3, the Nb_3Sn layer is clearly distinguishable from the Nb specimen and the Cu–Sn–Ti alloy. Thus, from such BEI micrographs, the mean thickness l of the Nb_3Sn layer was evaluated at each annealing time as follows:

$$l = A/w. \tag{1}$$

Here, w and A are the total length parallel to the α/Nb_3Sn interface and the total area of the Nb_3Sn layer, respectively, on the cross-section. The results of $T = 923$, 973, 1,023 and 1,053 K are plotted as open rhombuses, triangles, squares and circles, respectively, in Fig. 7. In this figure, the ordinate shows the logarithm of the thickness l, and the abscissa indicates the logarithm of the annealing time t. As can be seen in Fig. 7, the thickness l monotonically increases with increasing annealing time t, and the plotted points at each annealing temperature are located well on a straight line. Hence, l is expressed as a power function of t by the following equation:

$$l = k(t/t_0)^n. \tag{2}$$

Here, t_0 is unit time, 1 s. It is adopted to make the argument t/t_0 of the power function dimensionless. The proportionality coefficient k has the same dimension as the thickness l, but the exponent n is dimensionless. From the plotted points in Fig. 7, k and n were estimated by the least-squares method. The estimated values are shown in Fig. 7. Using these values of k and n, l was calculated as a function of t from Eq. 2. The results of $T = 923$, 973, 1,023 and 1,053 K are indicated as dashed-and-dotted, dotted, dashed and solid lines, respectively, in Fig. 7. The calculation shows that the growth rate of the Nb_3Sn layer monotonically increases with increasing annealing temperature.

The results of $T = 923$ and 1,053 K in Fig. 7 are plotted again as open circles with solid lines in Fig. 8a and b, respectively. As mentioned in Sect. ''Introduction'', the growth behavior of the Nb_3Sn layer was experimentally

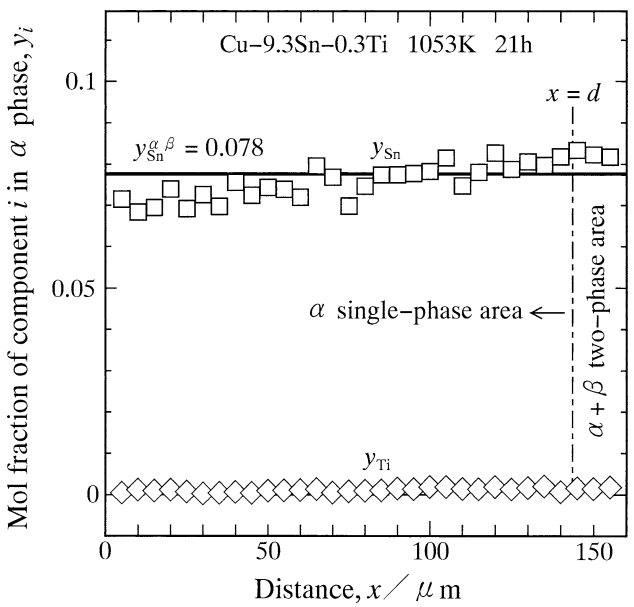

Fig. 6 Concentration profiles of Sn and Ti across the α single-phase area in Fig. 5

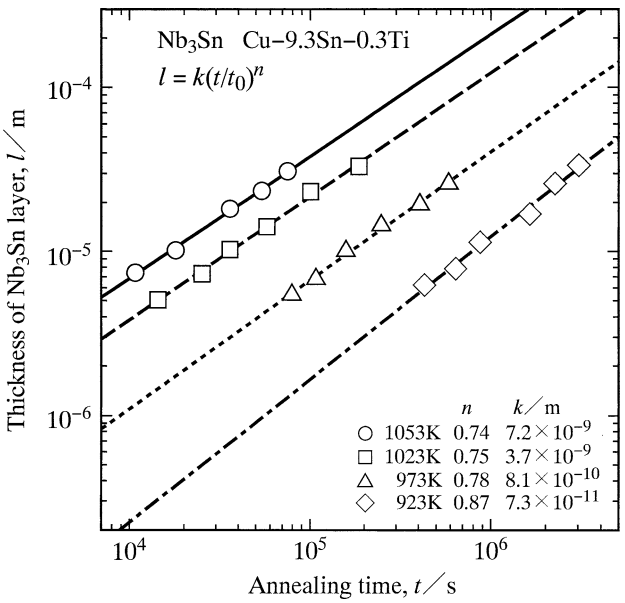

Fig. 7 The mean thickness l of the Nb_3Sn layer versus the annealing time t for the Cu–9.3Sn–0.3Ti diffusion couple at temperatures of $T = 923$, 973, 1,023 and 1,053 K shown as open rhombuses, triangles, squares and circles, respectively. Straight lines indicate the calculations from Eq. 2

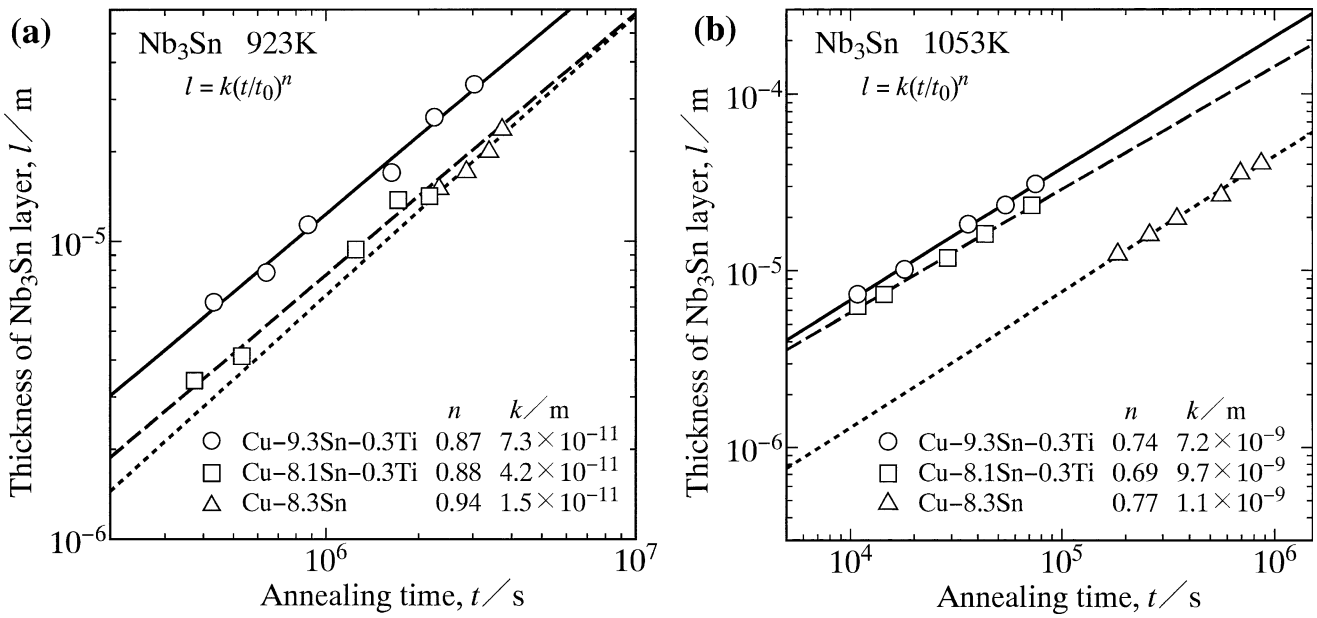

Fig. 8 The results in Fig. 7 are represented as open circles with solid lines for (**a**) T = 923 K and (**b**) T = 1,053 K. The results for the Cu–8.3Sn [14] and Cu–8.1Sn–0.3Ti [15] diffusion couples in previous studies are shown as open triangles and squares, respectively

observed also for the Cu–8.3Sn and Cu–8.1Sn–0.3Ti diffusion couples in previous studies [14, 15]. For simplicity, te type of diffusion couple is hereafter merely denoted by the composition of the bronze in the diffusion couple. The corresponding results of Cu–8.3Sn [14] and Cu–8.1Sn–0.3Ti [15] are represented as open triangles and squares, respectively, in Fig. 8. From the open triangles and squares, k and n in Eq. 2 were estimated by the least-squares method for Cu–8.3Sn and Cu–8.1Sn–0.3Ti, respectively. The results of Cu–8.3Sn and Cu–8.1Sn–0.3Ti as well as that of Cu–9.3Sn–0.3Ti are listed in Table 1. Using the values of k and n in this table, l was calculated as a function of t from Eq. 2. The results of Cu–8.3Sn and Cu–8.1Sn–0.3Ti are shown as dotted and dashed lines, respectively, in Fig. 8. According to the results of T = 923 K in Fig. 8a, the growth rate of the Nb_3Sn layer is slightly greater for Cu–9.3Sn–0.3Ti than for Cu–8.3Sn and Cu–8.1Sn–0.3Ti, but almost equivalent between Cu–8.3Sn and Cu–8.1Sn–0.3Ti. On the other hand, at T = 1,053 K in Fig. 8b, the growth rate is much greater for Cu–9.3Sn–0.3Ti and Cu–8.1Sn–0.3Ti than for Cu–8.3Sn, but mostly equivalent between Cu–9.3Sn–0.3Ti and Cu–8.1Sn–0.3Ti. According to the parameters k and n in Table 1, such a tendency is realized at the experimental annealing times also for T = 973 and 1,023 K. However, the difference of the growth rate gradually decreases with decreasing annealing temperature. Consequently, it is concluded that the addition of Ti with 0.3 at.% into the Cu–8Sn alloy accelerates the growth of the Nb_3Sn layer at T = 973–1,053 K. However, such an effect of Ti is negligible at T = 923 K. In contrast, the addition of Sn with 1 at.% into the Cu–8Sn–0.3Ti alloy lightly accelerates the growth at T = 923 K but hardly at T = 973–1,053 K. Thus, the acceleration effects of Sn and Ti are complementary each other.

Table 1 The values of k and n in Eq. 2 for the Cu–9.3Sn–0.3Ti (9S3T) diffusion couple

		9S3T	8S3T	8S
923 K	$k/10^{-11}$ m	7.3	4.2	1.5
	n	0.87	0.88	0.94
973 K	$k/10^{-10}$ m	8.1	2.0	0.42
	n	0.78	0.89	0.96
1,023 K	$k/10^{-9}$ m	3.7	1.2	0.36
	n	0.75	0.83	0.84
1,053 K	$k/10^{-9}$ m	7.2	9.7	1.1
	n	0.74	0.69	0.77

The corresponding results are also indicated for the Cu–8.3Sn (8S) and Cu–8.1Sn–0.3Ti (8S3T) diffusion couples in previous studies [14, 15]

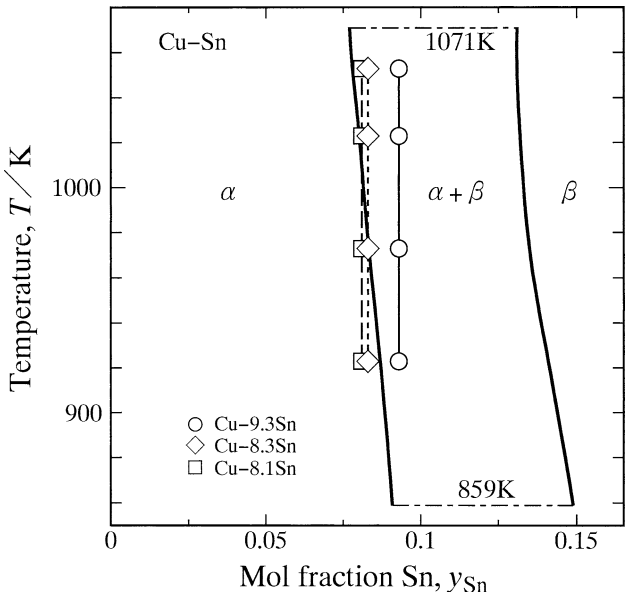

Fig. 9 The phase boundaries of the $\alpha + \beta$ two-phase region in a phase diagram of the binary Cu–Sn system [16]. The overall compositions of the Cu–9.3Sn, Cu–8.3Sn and Cu–8.1Sn alloys are shown as open circles, rhombuses and squares, respectively

As pointed out by Osamura et al. [13], Sn is the most predominant component governing the diffusion related to growth of Nb_3Sn during reactive diffusion between the bronze and Nb. The driving force for the diffusion is the activity of the relevant component. Thus, the activity a_{Sn} of Sn is the most important driving force for growth of Nb_3Sn [18]. Since the concentrations of Ti in the α and β phases are very small for both the Cu–8.1Sn–0.3Ti [15] and Cu–9.3Sn–0.3Ti alloys, these alloys are approximately considered as binary Cu–Sn alloys. The $\alpha + \beta$ two-phase region in a recent phase diagram of the binary Cu–Sn system [16] is shown in Fig. 9. In this figure, the ordinate indicates the temperature T, and the abscissa shows the mol fraction y_{Sn} of Sn. Furthermore, open squares, rhombuses and circles indicate the overall compositions of the Cu–8.1Sn, Cu–8.3Sn and Cu–9.3Sn alloys, respectively. According to the phase diagram in Fig. 9, the solubility $y_{Sn}^{\alpha\beta}$ of Sn in the α phase is 0.087, 0.083, 0.080 and 0.078 at T = 923, 973, 1,023 and 1,053 K, respectively. Thus, for the Cu–8.1Sn and Cu–8.3Sn alloys, the overall composition is located in the α single-phase region at T = 923–973 K but in the $\alpha + \beta$ two-phase region at T = 1,023–1,053 K. On the other hand, the overall composition of the Cu–9.3Sn alloy invariably lies in the $\alpha + \beta$ two-phase region at T = 923–1,053 K. In a binary Cu–Sn alloy with the $\alpha + \beta$ two-phase microstructure, the activity a_{Sn} is determined by the solubility $y_{Sn}^{\alpha\beta}$ at a given annealing temperature. At T = 1,023–1,053 K, the $\alpha + \beta$ two-phase microstructure is realized for the Cu–8.1Sn, Cu–8.3Sn and Cu–9.3Sn alloys, and hence a_{Sn} is equivalent among these alloys. On the other hand, at T = 923–973 K, the α single-phase microstructure is actualized for the Cu–8.1Sn and Cu–8.3Sn alloys, but the $\alpha + \beta$ two-phase microstructure is effectuated for the Cu–9.3Sn alloy. However, at T = 973 K, $y_{Sn}^{\alpha\beta}$ is equal to the overall composition of the Cu–8.3Sn alloy, and close to that of the Cu–8.1Sn alloy. Therefore, a_{Sn} is almost equivalent among the Cu–8.1Sn, Cu–8.3Sn and Cu–9.3Sn alloys at T = 973 K, but greater for the Cu–9.3Sn alloy than for the Cu–8.1Sn and Cu–8.3Sn alloys at T = 923 K. This is the reason why the growth rate of the Nb_3Sn layer is mostly equivalent between Cu–8.1Sn–0.3Ti and Cu–9.3Sn–0.3Ti at T = 973–1,053 K but greater for Cu–9.3Sn–0.3Ti than for Cu–8.1Sn–0.3Ti at T = 923 K. However, the growth rate is greater for Cu–8.1Sn–0.3Ti and Cu–9.3Sn–0.3Ti than for Cu–8.3Sn at T = 973–1,053 K. This is due to the influence of Ti on the growth rate.

As mentioned in Sect. ‘‘Microstructure’’, the growth of the Nb_3Sn layer occurs mainly into the Nb specimen but scarcely towards the Cu–Sn–Ti alloy. Such growth behavior of the Nb_3Sn layer was also observed for Cu–7.4Sn and Cu–7.5Sn–1Ti by Osamura et al. [13] and for Cu–8.3Sn [14] and Cu–8.1Sn–0.3Ti [15] in previous studies. Thus, the growth rate of the Nb_3Sn layer is predominantly determined by the migration rate of the Nb_3Sn/Nb interface. The migration of the Nb_3Sn/Nb interface towards the Nb specimen means that interdiffusion takes place much faster in the Nb_3Sn layer than in the Nb specimen [19, 20]. As a result, the migration is dominated by the interdiffusion across the Nb_3Sn layer. Influence of Ti on the growth of the Nb_3Sn layer was experimentally studied by Osamura et al. [13] Their result indicates that the grain size of the Nb_3Sn layer is markedly decreased by the addition of Ti with 1 at.% into the Cu–7Sn alloy. The interdiffusion will be accelerated by the grain boundary diffusion along grain boundaries in the Nb_3Sn layer with fine grains. Consequently, the growth rate of the Nb_3Sn layer becomes greater for Cu–7.5Sn–1Ti than for Cu–7.4Sn. Such a mechanism of the acceleration is valid for explanation of the difference between the growth rates of Nb_3Sn for Cu–8.3Sn and Cu–8.1Sn–0.3Ti [14, 15]. However, the kinetic information of Nb_3Sn is not available for Cu–9.3Sn. Thus, it is not possible to compare the growth behavior of Nb_3Sn for Cu–9.3Sn–0.3Ti with that of Nb_3Sn for Cu–9.3Sn. Nevertheless, the addition of Ti with 0.3 at.% into a Cu–9.3Sn alloy will accelerate the growth of Nb_3Sn. This is the reason why the growth rate of the Nb_3Sn layer is greater for Cu–9.3Sn–0.3Ti and Cu–8.1Sn–0.3Ti than for Cu–8.3Sn at T = 973–1,053 K as shown in Table 1 and Fig. 8b. At T = 923 K in Fig. 8a, however, the growth rate is nearly equivalent between Cu–8.1Sn–0.3Ti and Cu–8.3Sn. The equivalency of the growth rate for the latter diffusion couples was extensively discussed in a previous study [15].

Growth behavior of α single-phase area

As mentioned in Sect. ''Microstructure'', the α single-phase area is formed in the Cu–9.3Sn–0.3Ti alloy neighboring the Nb_3Sn layer in the diffusion couple during annealing. As shown in Fig. 5, the base-line of the α single-phase area is almost parallel to the α/Nb_3Sn interface, though the β phase is rather irregular in morphology. From the BEI micrograph like Fig. 5, the mean thickness d of the α single-phase area was measured metallographically. As shown in Fig. 9, however, the overall composition of the Cu–9.3Sn alloy is not much greater than the solubility $y_{Sn}^{\alpha\beta}$ at T = 923 K. Thus, at this temperature, the volume fraction of the β phase is very small, and the measurement of d cannot be carried out reliably. The results of T = 973, 1,023 and 1,053 K are shown as open triangles, squares and circles, respectively, in Fig. 10. In this figure, the ordinate indicates the logarithm of the thickness d, and the abscissa shows the logarithm of the annealing time t. As can be seen, d monotonically increases with increasing value of t, and the plotted points at each annealing temperature lie well on a straight line. Thus, d is expressed as a power function of t by the equation

$$d = k_d(t/t_0)^p. \quad (3)$$

Here, like Eq. 2, the proportionality coefficient k_d has the same dimension as d, but the exponent p is dimensionless. From the plotted points in Fig. 10, k_d and p were estimated by the least-squares method. The estimated values are indicated in Fig. 10. Using these values of k_d and p, d was calculated as a function of t from Eq. 3. The results of T = 973, 1,023 and 1,053 K are shown as dotted, dashed and solid lines, respectively, in Fig. 10. The calculation indicates that the growth rate of the α single-phase area increases with increasing annealing temperature.

Rate-controlling process

The values of the exponent n for Cu–9.3Sn–0.3Ti are plotted as open circles against the annealing temperature T in Fig. 11. Here, the ordinate and the abscissa show n and T, respectively. In this figure, the corresponding results of Cu–8.3Sn [14] and Cu–8.1Sn–0.3Ti [15] are represented as open triangles and squares, respectively. When the interdiffusion across the Nb_3Sn layer is the rate-controlling process for the migration of the Nb_3Sn/Nb interface and the volume diffusion of each component in the Nb_3Sn layer governs the interdiffusion, n is equivalent to 0.5. On the other hand, n becomes equal to unity for the migration of the Nb_3Sn/Nb interface controlled by the interface reaction [21]. According to the result for Cu–9.3Sn–0.3Ti in Fig. 11, n is close to unity at T = 923 K, but decreases to 0.8–0.7 at T = 973–1,053 K. Consequently, the migration of the Nb_3Sn/Nb interface is predominantly controlled by the interface reaction at T = 923 K, but the interdiffusion as well as the interface reaction contributes to the

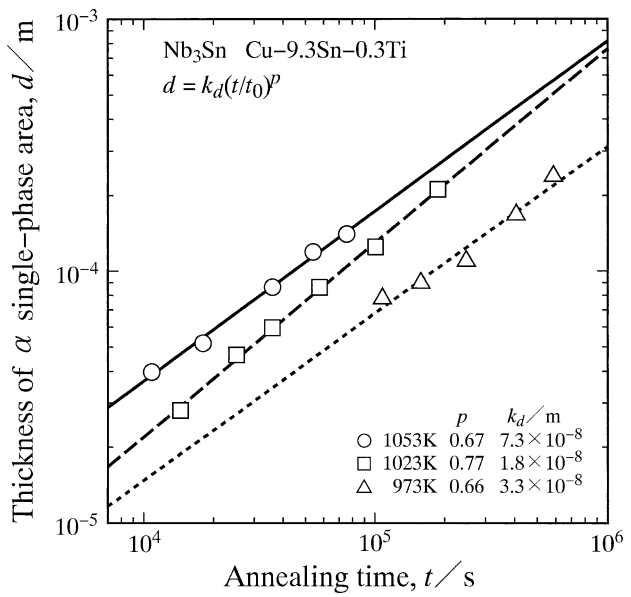

Fig. 10 The mean thickness d of the α single-phase area versus the annealing time t for the Cu–9.3Sn–0.3Ti diffusion couple at temperatures of T = 973, 1,023 and 1,053 K shown as open triangles, squares and circles, respectively. Straight lines indicate the calculations from Eq. 3

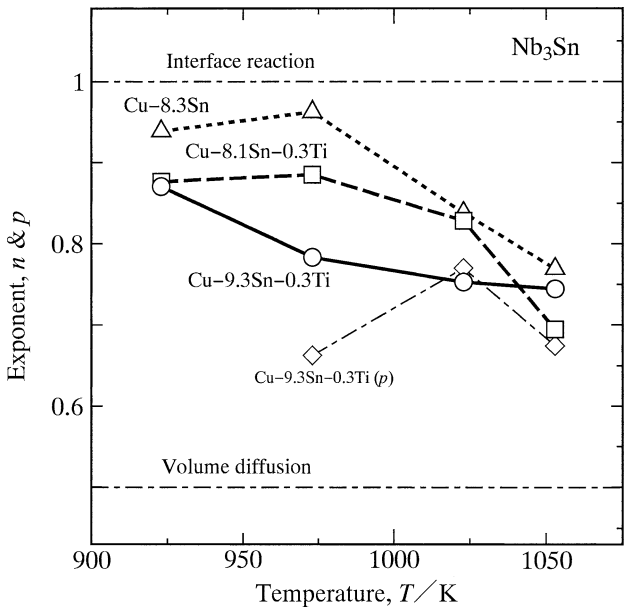

Fig. 11 The exponent n versus the annealing temperature T for the result in Fig. 7 shown as open circles. The results for the Cu–8.3Sn [14] and Cu–8.1Sn–0.3Ti [15] diffusion couples in previous studies are indicated as open triangles and squares, respectively. Open rhombuses show the values of p in Fig. 10

rate-controlling process at T = 973–1,053 K. Similar temperature dependence of the rate-controlling process is recognized also for Cu–8.3Sn and Cu–8.1Sn–0.3Ti. For the latter diffusion couples, however, the interface reaction is still the rate-controlling process even at T = 973 K.

Tin-base alloys are widely used as solder materials in electronic industry. When the Sn-base solder alloy is interconnected with a certain conductor alloy, relevant intermetallic compounds are formed at the interconnection due to reactive diffusion during soldering. Such intermetallic compounds gradually grow during heating under usual energization conditions. Since these intermetallic compounds are brittle and possess high electrical resistivities, their growth deteriorates the electrical and mechanical properties of the interconnection. In order to examine the growth behavior of the intermetallic compounds during energization heating, the kinetics of the reactive diffusion between Sn-base solders and various conductor metals was experimentally observed in previous studies [22–35]. As to the reactive diffusion in the Sn/(Au–Ni) system [34], sandwich Sn/(Au–Ni)/Sn diffusion couples were prepared from pure Sn and binary Au–Ni alloys with Sn concentrations of 27 and 46 at.% by a diffusion bonding technique, and then isothermally annealed at T = 433–473 K. Here, the notation A/(B–C) means that reactive diffusion occurs between a pure A metal and a binary B–C alloy at appropriate annealing temperatures. During annealing, the $AuNiSn_8$ layer distributed with small particles of Ni_3Sn_4 is formed at each Sn/(Au–Ni) interface in the diffusion couple, and grows mainly into Sn. Also in this case, the mean thickness l of the $AuNiSn_8$ layer is expressed as a power function of the annealing time t by Eq. 2. For Au–46Ni, the exponent n is close to 0.5 at T = 453–473 K, and increases to 0.7 at T = 433 K. Thus, the growth of the $AuNiSn_8$ layer is controlled by the volume diffusion of the constituent components in each phase at T = 453–473 K, but the interface reaction at the migrating Sn/$AuNiSn_8$ interface as well as the volume diffusion contributes to the rate-controlling process at T = 433 K. Similar temperature dependence of the rate-controlling process was observed also for the reactive diffusion in the Ni/(Sn–Au) system at T = 433–473 K using a sandwich (Sn–5Au)/Ni/(Sn–5Au) diffusion couple [35]. The annealing temperature is much lower for Au–46Ni and Sn–5Au than for Cu–9.3Sn–0.3Ti, Cu–8.1n–0.3Ti and Cu–8.3Sn. Nevertheless, among these diffusion couples, the common tendency is recognized for the temperature dependence of the rate-controlling process.

In Fig. 11, the values of the exponent p for Cu–9.3Sn–0.3Ti are also shown as open rhombuses. If the transport of Sn from the $\alpha + \beta$ two-phase area to the Nb_3Sn layer is controlled by the volume diffusion across the α single-phase area, p is equal to 0.5. On the other hand, p is equivalent to unity for the transport governed by the interface reaction at the α/β interface and/or that at the α/Nb_3Sn interface. According to the result in Fig. 11, p takes values of 0.7–0.8 at T = 973–1,053 K. This means that the interface reaction as well as the volume diffusion contributes to the rate-controlling process for the transport of Sn. Unlike the exponent n, however, there is no systematic temperature dependence for the exponent p. As mentioned in Sect. ''Microstructure'', the equilibrium composition is not realized for the β phase in the $\alpha + \beta$ two-phase area during annealing. In such a case, the local equilibrium will not be necessarily actualized at the α/β interface. Hence, the interface reaction at the α/β interface may affect the dissolution of the β phase into the α phase during growth of the α single-phase area. On the other hand, the interface reaction at the Nb_3Sn/Nb interface plays an important role for the growth of the Nb_3Sn layer as mentioned earlier. This implies that the interface reaction at the stationary α/Nb_3Sn interface may not be completely negligible. Consequently, it is anticipated that the transport of Sn is controlled by the interface reactions at the α/β and α/Nb_3Sn interfaces as well as the volume diffusion.

The values of k for Cu–9.3Sn–0.3Ti are plotted against the reciprocal of T as open symbols in Fig. 12. The temperature dependence of k is usually expressed by the equation [24]

$$k = k_0 \exp(-Q_k/RT). \tag{4}$$

Here, k_0 is the pre-exponential factor, Q_k is the activation enthalpy, and R is the gas constant. As previously

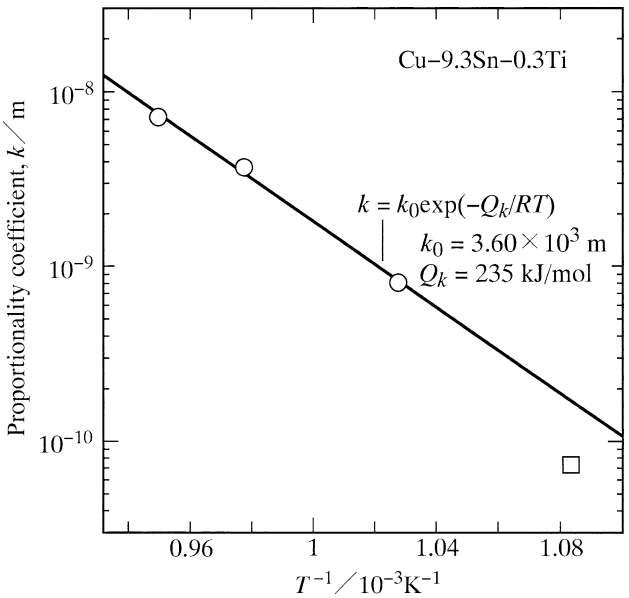

Fig. 12 The proportionality coefficient k versus the reciprocal of the annealing temperature T for the Cu–9.3Sn–0.3Ti diffusion couple. The results of T = 973–1,053 K are shown as open circles, and that of T = 923 K is indicated as an open square

mentioned, the interface reaction at the migrating Nb_3Sn/Nb interface is the rate-controlling process at T = 923 K, but the interdiffusion across the Nb_3Sn layer as well as the interface reaction contributes to the rate-controlling process at T = 973–1,053 K. However, the exponent n is almost constant at T = 973–1,053 K as shown in Fig. 11. This implies that the ratio between the contributions of the interdiffusion and the interface reaction to the rate-controlling process is nearly constant independent of the annealing temperature at T = 973–1,053 K. Thus, in Fig. 12, the values of k at T = 973–1,053 K are shown as open circles, and that of k at T = 923 K is indicated as an open square. Estimating k_0 and Q_k in Eq. 4 only from the open circles by the least-squares method, we obtain $k_0 = 3.60 \times 10^3$ m and Q_k = 235 kJ/mol. From Eq. 4, k was calculated as a function of T using these values of k_0 and Q_k. The result is shown as a solid line in Fig. 12. As mentioned above, the interdiffusion and the interface reaction contribute to the rate-controlling process at T = 973–1,053 K. Therefore, $k_0 = 3.60 \times 10^3$ m and Q_k = 235 kJ/mol correspond to the pre-exponential factor and the activation enthalpy, respectively, for the mixed rate-controlling process. In such a case, there exist no clear physical meanings for k_0 and Q_k. Nevertheless, as can be seen in Fig. 12, the open circles lie well on the solid line. On the other hand, at T = 923 K, the interface reaction is the rate-controlling process and thus the bottleneck against the migration of the Nb_3Sn/Nb interface. As a result, the growth of the Nb_3Sn layer decelerates, and the open square lies below the solid line in Fig. 12.

The kinetics of reactive diffusion was experimentally observed for various alloy systems by many investigators [36–47]. According to the observation, however, the reactive diffusion is purely controlled by volume diffusion for most of the alloy systems. This means that the square of the thickness l of the compound layer is proportional to the annealing time t as follows.

$$l^2 = Kt \tag{5}$$

The relationship of Eq. 5 is usually called the parabolic relationship. Here, K is the parabolic coefficient. The temperature dependence of K is expressed by the following equation of the same formula as Eq. 4.

$$K = K_0 \exp(-Q_K/RT) \tag{6}$$

Here, K_0 and Q_K are the pre-exponential factor and the activation enthalpy, respectively. The values of Q_K are reported for various alloy systems as follows: Q_K = 106 kJ/mol for the Pd–Sn system [29], Q_K = 82–256 kJ/mol for the Al–Cu system [39], Q_K = 192 kJ/mol for the Co–Si system [42], Q_K = 130–254 kJ/mol for the Si–V system [43], Q_K = 220–360 kJ/mol for the Mo–Si system [44], Q_K = 226–281 kJ/mol for the Al–Fe system [37, 47], etc. K is the proportionality coefficient for the power function of t with n = 1 in Eq. 5, but k is that for the power function of t with n = 0.74–0.78 in Eq. 2. Since there is a small difference between the values of n for K and k, Q_k may not be directly compared with Q_K. Nevertheless, Q_k = 235 kJ/mol is located well within the values of Q_K reported for various alloy systems [36–47]. This implies that the volume diffusion plays an important role in the mixed rate-controlling process for growth of Nb_3Sn in the bronze method.

Conclusions

The kinetics of the reactive diffusion between the ternary Cu–9.3 at.% Sn–0.3 at.% Ti alloy and pure Nb was experimentally examined using the sandwich (Cu–Sn–Ti)/Nb/(Cu–Sn–Ti) diffusion couple prepared by a diffusion bonding technique. The diffusion couple was isothermally annealed in the temperature range between T = 923 and 1,053 K for various times up to 843 h. In this temperature range, the $\alpha + \beta$ two-phase microstructure is realized in the Cu–9.3Sn–0.3Ti alloy. Here, α is the primary solid-solution phase of Cu with the fcc structure, and β is the intermediate phase with the bcc structure. During annealing, the Nb_3Sn compound with the A-15 type crystal structure is produced as a layer along the (Cu–Sn–Ti)/Nb interface in the diffusion couple. The Nb_3Sn layer grows mainly into Nb but scarcely towards the Cu–Sn–Ti alloy. This means that the growth of the Nb_3Sn layer is governed by the migration of the Nb_3Sn/Nb interface. The mean thickness of the Nb_3Sn layer is expressed as a power function of the annealing time. The exponent of the power function is nearly equal to unity at T = 923 K, and takes values of 0.8–0.7 at T = 973–1,053 K. Thus, the interface reaction at the migrating Nb_3Sn/Nb interface is the rate-controlling process for the growth of the Nb_3Sn layer at T = 923 K, and the interdiffusion across the Nb_3Sn layer as well as the interface reaction contributes to the rate-controlling process at T = 973–1,053 K. Recently, the Cu–9.3Sn–0.3Ti alloy with the $\alpha + \beta$ two-phase microstructure is preferentially used to manufacture the superconducting Nb_3Sn composite-wire by the bronze method. On the other hand, for a conventional Cu–8.1Sn–0.3Ti alloy, the $\alpha + \beta$ two-phase microstructure is effectuated at T > 1,000 K, but the α single-phase microstructure is actualized at T < 1,000 K [15]. Since the concentration y_{Sn} of Sn is higher for the β phase than for the α phase, the amount of Sn supplied to Nb_3Sn is greater for the $\alpha + \beta$ two-phase microstructure than for the α single-phase microstructure. Hence, we may expect that the growth of the Nb_3Sn layer is accelerated by the β phase in the Cu–Sn–Ti alloy. Except the effect of Ti,

however, the growth rate of the Nb_3Sn layer is principally controlled by the activity a_{Sn} of Sn in the α phase as pointed out in a previous study [18]. For the α + β two-phase microstructure, a_{Sn} is determined by the solubility $y_{Sn}^{\alpha\beta}$ of Sn in the α phase but independent of the volume fraction of the β phase. Therefore, influence of the β phase on the growth rate of the Nb_3Sn layer is negligible as long as the concentration y_{Sn}^{α} of Sn in the α phase is close to $y_{Sn}^{\alpha\beta}$. Since y_{Sn}^{α} of the Cu–8.1Sn–0.3Ti alloy is smaller than $y_{Sn}^{\alpha\beta}$ at $T = 923$ K, however, the growth rate of the Nb_3Sn layer is greater for the Cu–9.3Sn–0.3Ti alloy than for the Cu–8.1Sn–0.3Ti alloy. Consequently, at temperatures around $T = 900$ K, the addition of Sn with 1 at.% into the conventional Cu–8Sn–Ti alloy accelerates the growth of Nb_3Sn during reactive diffusion in the bronze method.

Acknowledgements The authors are grateful to Messrs. S. Meguro, K. Wada and H. Sakamoto at Furukawa Electric Co., Ltd., Japan for stimulating discussions. The present study was supported by Furukawa Electric Co., Ltd. The study was also partially supported by a Grant-in-Aid for Scientific Research from the Ministry of Education, Culture, Sports, Science and Technology of Japan.

References

1. Kaufmann AR, Pickett JJ (1970) Bull Am Phys Soc 15:838
2. Suenaga M, Sampson WB (1971) Appl Phys Lett 18:584
3. Tachikawa K, Yoshida Y, Rinderer L (1972) J Mater Sci 7:1154
4. Suenaga M, Sampson WB (1972) Appl Phys Lett 20:443
5. Farrell HH, Gilmer GH, Suenaga M (1974) J Appl Phys 45:4025
6. Farrell HH, Gilmer GH, Suenaga M (1975) Thin Solid Films 25:253
7. Dew-Hughes H, Luhman TS, Suenaga M (1976) Nucl Technol 29:268
8. Murase S, Koike Y, Shiraki H (1978) J Appl Phys 49:6020
9. Kwasnitza K, Narlikar AV, Nissen HU, Salathé D (1980) Cryogenics 715
10. Upadhyay P, Samanta SB, Narlikar AV (1981) Mat Res Bull 16:741
11. Reddi BV, Raghavan V, Ray S, Narlikar AV (1983) J Mater Sci 18:1165
12. Cheng CC, Verhoeven JD (1988) J Less-Com Met 139:15
13. Osamura K, Ochiai S, Kondo S, Namatame M, Nosaki M (1986) J Mater Sci 21:1509
14. Muranishi Y, Kajihara M (2005) Mater Sci Eng A 404:33
15. Hayase T, Kajihara M (2006) Mater Sci Eng A 433:83
16. Massalski TB, Okamoto H, Subramanian PR, Kacprzak L (1990) Binary alloy phase diagrams, vol 2. ASM International, Materials Park, Ohio, p 1482
17. Kajihara M, Lim C-B, Kikuchi M (1993) ISIJ Int 33:498
18. Yamashina T, Kajihara M (2006) Mater Trans 47:829
19. Jost W (1960) Diffusion of solids, liquids, gases. Academic Press, New York, p 68
20. Kajihara M (2004) Acta Mater 52:1193
21. Sutton AP, Balluffi RW (1995) Interfaces in crystalline materials. Oxford Science Publications, Clarendon Press, Oxford, p 603
22. Kajihara M, Yamada T, Miura K, Kurokawa N, Sakamoto K (2003) Netsushori 43:297
23. Yamada T, Miura K, Kajihara M, Kurokawa N, Sakamoto K (2004) J Mater Sci 39:2327
24. Yamada T, Miura K, Kajihara M, Kurokawa N, Sakamoto K (2005) Mater Sci Eng A 390:118
25. Kajihara M, Takenaka T (2007) Mater Sci Forum 539–543:2473
26. Suzuki K, Kano S, Kajihara M, Kurokawa N, Sakamoto K (2005) Mater Trans 46:969
27. Mita M, Kajihara M, Kurokawa N, Sakamoto K (2005) Mater Sci Eng A 403:269
28. Takenaka T, Kano S, Kajihara M, Kurokawa N, Sakamoto K (2005) Mater Sci Eng A 396:115
29. Takenaka T, Kajihara M, Kurokawa N, Sakamoto K (2005) Mater Sci Eng A 406:134
30. Takenaka T, Kano S, Kajihara M, Kurokawa N, Sakamoto K (2005) Mater Trans 46:1825
31. Mita M, Miura K, Takenaka T, Kajihara M, Kurokawa N, Sakamoto K (2006) Mater Sci Eng B 126:37
32. Takenaka T, Kajihara M (2006) Mater Trans 47:822
33. Takenaka T, Kajihara M, Kurokawa N, Sakamoto K (2006) Mater Sci Eng A 427:210
34. Yato Y, Kajihara M (2006) Mater Sci Eng A 428:276
35. Yato Y, Kajihara M (2006) Mater Trans 47:2277
36. Peterson NL, Ogilvie RE (1960) Trans Met Soc AIME 218:439
37. Shibata K, Morozumi S, Koda S (1966) J Jpn Inst Met 30:382
38. Hirano K, Ipposhi Y (1968) J Jpn Inst Met 32:815
39. Funamizu Y, Watanabe K (1971) Trans JIM 12:147
40. Onishi M, Fujibuchi H (1975) Trans JIM 16:539
41. Tortorici PC, Dayananda MA (1999) Met Mater Trans A 30A: 545
42. van Dal MJH, Huibers DGGM, Kodentsov AA, van Loo FJJ (2001) Intermetallics 9:409
43. Milanese C, Buscaglia V, Maglia F, Anselmi-Tamburini U (2002) Acta Mater 50:1393
44. Hayashi T, Ito K, Numakura H (2005) Intermetallics 13:93
45. Tanaka Y, Kajihata M, Watanabe Y (2007) Mater Sci Eng A 445–446:355
46. Kajihara M, Sakama T (2007) Proc 13th Symp Microjoining Assembly Tech Electronics. Microjoining Commission, Yokohama, 187
47. Naoi D, Kajihara M (2007) 5. Mater Sci Eng A 459:375